Published in IET Microwaves, Antennas & Propagation
Received on 1st April 2010
Revised on 25th August 2010
doi: 10.1049/iet-map.2010.0132

ISSN 1751-8725

Microwave modelling of radio frequency microelectromechanical rotary switches

S. Pranonsatit[1] *A.S. Holmes*[2] *S. Lucyszyn*[2]

[1]*Department of Electrical Engineering, Faculty of Engineering, Kasetsart University, Bangkok, Thailand*
[2]*Department of Electrical and Electronic Engineering, Imperial College London, London SW7 2AZ, UK*
E-mail: s.lucyszyn@imperial.ac.uk

Abstract: In this study, both full 3D electromagnetic and equivalent circuit modelling of a radio frequency microelectromechanical systems (RF MEMS) single-pole eight-throw rotary switch are reported for the first time. Excellent agreement has been achieved between measurements and modelled performance for frequencies up to 12 GHz. In order to validate the effectiveness of the modelling, a 2-bit true time delay phase shifter having a centre frequency of 2 GHz has been demonstrated. The traditional topology of the switched delay line was adopted with two rotary switches employed for signal routing. This phase shifter represents the first ever application of any RF MEMS rotary switch. It is shown that the switch model can accurately predict the measured performance of the phase shifter, without the need for adding new circuit elements or tweaking of model parameters. The low measured root mean square deviations of insertion phase from the predicted responses increase as 1.3°, 1.9°, 2.5° and 3.4° when the phase states are stepped through 0°, 90°, 180° and 270°, respectively.

1 Introduction

Recently, the authors introduced a unique radio frequency microelectromechanical systems (RF MEMS) [1] single-pole eight-throw (SP8T) rotary switch, based on the axial-gap wobble motor principle [2]. With reference to Fig. 1, the switch stator has an input coplanar waveguide (CPW) feed line (labelled 'IN') that extends up to the central bearing, and eight output CPW lines ('OUT1' etc.) that terminate at points around the periphery. Connection between the input line and a particular output line occurs via the tilted metal rotor that is rotated until it forms an ohmic contact with the required output line. The rotor is actuated electrostatically via drive electrodes on the stator. The mechanical design, fabrication processing and measurement characteristics of the switch were previously discussed in detail [2].

This study reports on the microwave modelling of the RF MEMS SP8T rotary switch and its validation with a 2-bit true time delay (TTD) phase shifter. To the authors' knowledge, this represents the first reported application of a truly rotary RF MEMS switch.

2 Rotary switch modelling

Two modelling strategies were adopted for characterisation of the rotary switch: 3D electromagnetic and equivalent circuit modelling. With the former, ANSOFT's high-frequency structure simulator (HFSS^{TM}) software was employed to predict the performance of the 3D structure. With the latter, AWR's Microwave Office software was employed to create an accurate equivalent circuit model for the switch, using traditional parameter extraction techniques. Fig. 1 serves as a useful illustration of the basic structure of the switch. The rotor shown, which is in the form of a cartwheel with eight spokes, is one of two designs (the other being a solid disc).

2.1 Full 3D electromagnetic modelling

A virtual 3D structure was constructed for the rotary switch; composing of a substrate, stator, CPW feed lines and rotor. The material specifications, geometry and dimensions correspond to those of the real switch. The substrate is made of 500 μm-thick HOYA Co. amorphous synthetic quartz, having a relative permittivity of 3.58 and loss tangent of 0.12×10^{-4}. The dielectric spacer is made of SU-8, with values of 4.2 and 0.08 for the relative permittivity and loss tangent, respectively [3].

The structural metal for both the stator and rotor was electroplated nickel (used extensively in MEMS), with an additional top layer of gold. An important factor that could not be neglected was the ferromagnetic nature of nickel. The default relative permeability value in HFSS^{TM}, as well as in many microwave textbooks, is $\mu_r = 600$. However, this value is applicable only at low frequencies. To determine the permeability of our deposited nickel at microwave frequencies, three different lengths of pure nickel transmission line were fabricated and characterised. The results were compared with HFSS^{TM} models of the lines, and the model μ_r was adjusted for best fit. This parameter extraction technique gave a value of $\mu_r = 8$, which falls within the expected range of 3–9 identified in literature surveys [4]. As expected, subsequent HFSS^{TM} simulations showed that major improvements in the overall

© The Institution of Engineering and Technology 2011

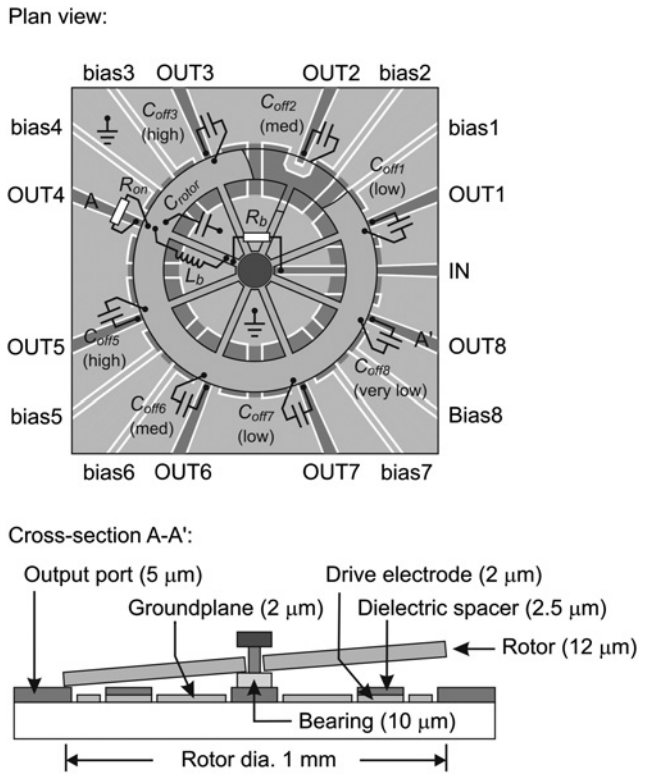

Fig. 1 *Plan and side views for the basic switch making contact to OUTPUT 4, with intrinsic lumped elements shown*

Layer thicknesses are shown in brackets

RF performance of the phase shifter could be achieved by replacing nickel with copper.

The 3 × 3 mm^2 virtual 3D model for the switch is shown in Fig. 2. All dimensions were transposed from the original mask layout designs. One input wave port and eight output wave ports were assigned, with their location and size defined by following HFSS^{TM} recommendations. Finally, a radiation boundary was used for the top and side walls, and a stainless steel bottom boundary was introduced to represent the chuck of the RF on-wafer probe station. This boundary layer was separated from the substrate by a 500 μm-thick air layer representing the perforated printed circuit board (PCB) used in practice.

Fig. 3 compares the predicted and measured ON-state insertion losses for a switch with a cartwheel rotor. These data show intrinsic insertion loss after correction for impedance mismatches within the standard 50 Ω reference impedance measurement environment. The correction was made by importing 2-port *S*-parameter files into AWR's Microwave Office and selecting GMax (i.e. maximum available gain or MAG) as the 'measurement type'.

The model predictions for OUTPUT 1 include two scenarios, one where the output is aligned to a spoke on the rotor, and the other where the output lies between two spokes. The misaligned case shows slightly higher insertion loss, because of increased series inductance, although the difference is negligible below about 12 GHz. The disc rotor was found to give slightly worse ON-state insertion loss, indicating that the benefit of lower series inductance with the disc was more than offset by its higher shunt capacitance.

The OFF-state isolation between the input port and unselected output ports was also examined within a 50 Ω reference impedance environment. With reference to Figs. 1 and 2, the capacitive coupling between the input feed line and rotor is at its lowest when the rotor makes contact with OUTPUT 4 or OUTPUT 5. In contrast, this capacitive coupling will be greatest when the rotor makes contact with OUTPUT 1 or OUTPUT 8. The predicted isolation between the input port and all non-selected output ports is shown in Fig. 4, when the worst-case isolation condition is chosen (e.g. with OUTPUT 1 selected).

In addition, a typical measured isolation response, taken from Fig. 10 in reference [2], is also included in order to show how the general frequency behaviours match. As expected, the best isolation performance is obtained with OUTPUT 5, followed by OUTPUTS 6, 4, 7, 3 and 2, in that order. OUTPUT 8 does not have the same frequency profile as the rest, because of its position relative to the input line. The isolation at high frequencies was improved by a few dB with the disc rotor, when compared with the cartwheel rotor, because of its extra shunt capacitance.

2.2 Equivalent circuit modelling

Intrinsic lumped-element equivalent circuit models for the rotary switch are shown in Fig. 5, with reference planes located at the centre of the stator (i.e. base of the bearing) and the output contact point on the stator. During the RF

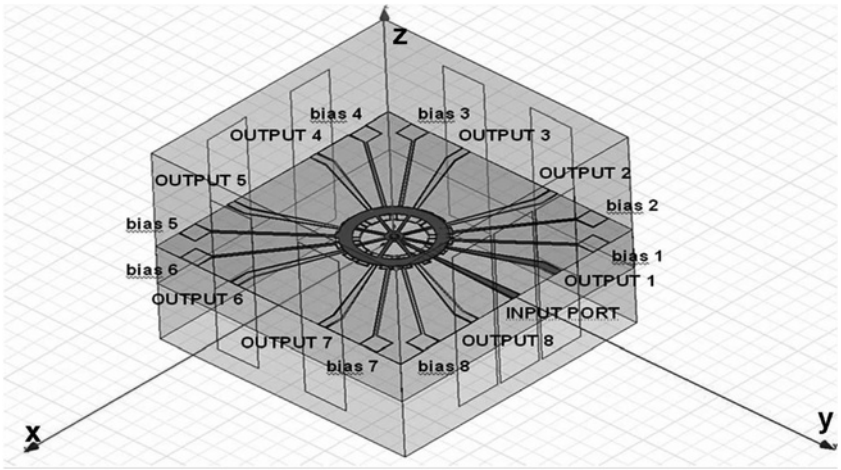

Fig. 2 *Isometric view of the HFSS^{TM} model for the switch having a cartwheel rotor, switched to OUTPUT 1, with radial spokes perfectly aligned to all the output lines*

© The Institution of Engineering and Technology 2011

doi: 10.1049/iet-map.2010.0132

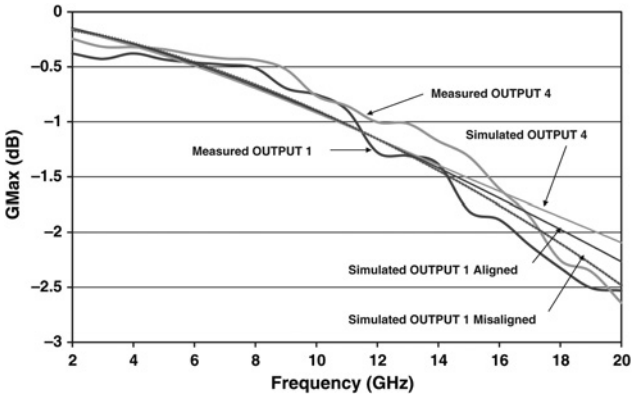

Fig. 3 *Predicted and measured GMax performances at different contact positions and cartwheel rotor orientations*

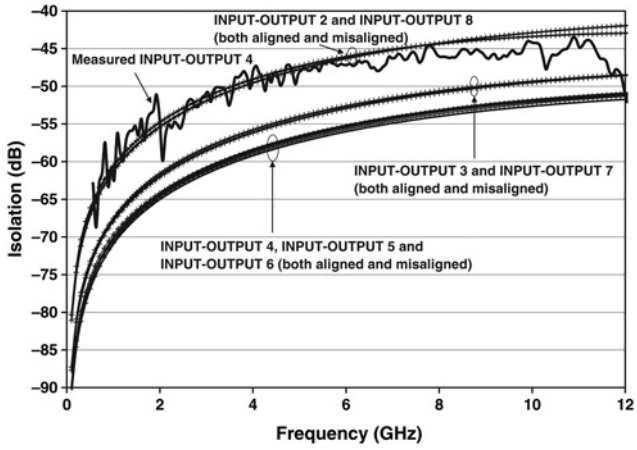

Fig. 4 *Predicted isolation performance with a cartwheel rotor, when switched to OUTPUT 1, between the input port and all other output ports*

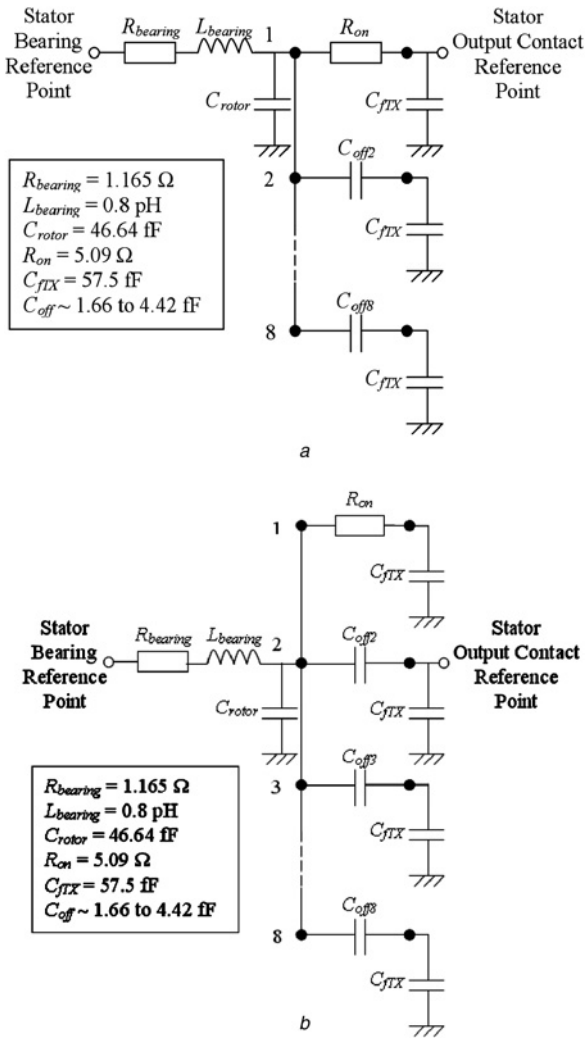

Fig. 5 *Intrinsic lumped-element equivalent circuit models for the SP8T switched to OUTPUT 1*

a ON state
b OFF state at OUTPUT 2

measurements, the probe tips were located 1.1 mm away from the rotor. Therefore the complete extrinsic model of the measured devices includes 1.5 mm of input feed line and 1.1 mm of feed line on each of the eight output contacts.

Here, a simple generic transmission line model (TLINP) was used, having frequency-dependent insertion phase and power attenuation characteristics. The model is based on a 50 Ω line, having an effective relative permittivity of 2.3 and attenuation coefficient of 0.09 dB/mm, with 10 GHz as the scaling frequency. These parameters were extracted from measurements of long 50 Ω test lines, located on the same substrate as the switch.

The corresponding measured and resulting extrinsic equivalent circuit model frequency responses, for both magnitude and phase angle of the forward voltage wave transmission and input voltage wave reflection coefficients, are shown in Fig. 6. It can be seen that there is an excellent fit for this arbitrary example where OUTPUT 4 is selected; the same level of fit can also be found with all other rotor position outputs.

As expected, it was found that all but the OFF-state or isolation capacitances, C_{off}, are independent of switch state and rotor position. The resulting fixed parameter-extracted values are shown in Fig. 5. The high average level of R_{on} can be explained by the poor surface roughness measured using earlier profiler measurements [2] and exacerbated by the inherent skin effect losses found at microwave frequencies. However, it should be noted that this is a fabrication process issue that can be easily rectified by process optimisation.

With the OFF state, the same fixed parameter values are used, as with the ON state, but the lumped elements themselves are simply reconfigured for the new switch state and rotor position. The corresponding measured and resulting extrinsic equivalent circuit model frequency responses are shown in Fig. 7. Once again, OUTPUT 4 was chosen as the ON-state output, whereas three different OFF-state outputs were characterised. It can be seen that the OFF-state models produce excellent fits with their corresponding measurements, for the same fixed values used with the equivalent circuit model elements in both ON and OFF states. Indeed, it has been found that this equivalent circuit model is robust and works very well in any switch state or rotor position.

The ON-state resistance can be reduced with an improved metal and its deposition processing (e.g. replacing the nickel layer that gives structural support to the rotor with copper), by applying a higher contact force (e.g. by increasing the size of the actuation electrode and/or the electrostatic bias voltage, although both these solutions are undesirable) and/or by reducing the surface roughness of the gold ohmic contacts. The nickel and gold deposition

© The Institution of Engineering and Technology 2011

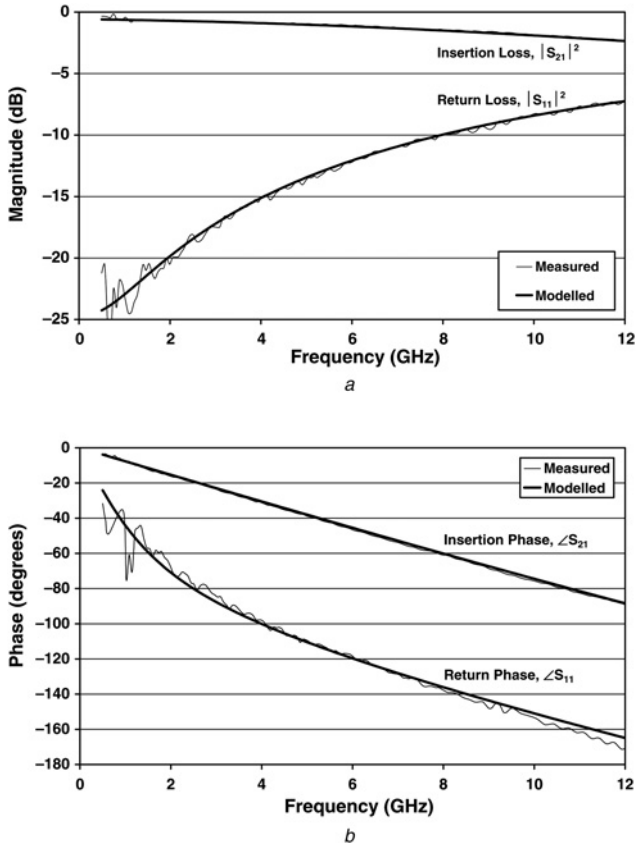

Fig. 6 *Measured and modelled switch results in ON state when OUTPUT 4 is selected*

a Magnitude
b Phase

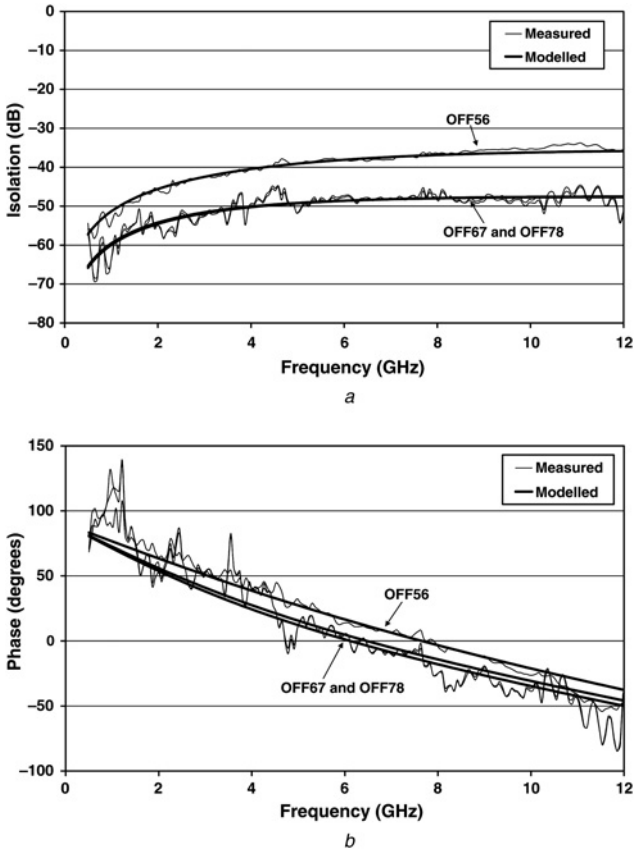

Fig. 7 *Measured and modelled switch results in OFF states when OUTPUT 4 is selected*

a Magnitude
b Phase

processes used for this work were developed to avoid the problem of plating underneath the photoresist mask layer (as a result of chemical reactions that can take place between the electroplating solution and photoresist). Unfortunately, the gold electroplating solution resulted in poor surface roughness and large asperities at the ohmic contacts. However, a newly developed gold electroplating solution is now commercially available that has only a small effect on the photoresist. As a result, the gold deposition process can be optimised to greatly improve the surface finish. The OFF-state capacitances can be reduced by increasing the height of the bearing and hence tilt angle.

3 Experimental RF MEMS TTD phase shifter demonstrator

Using the equivalent circuit models developed in Section 2, a 2-bit TTD phase shifter was investigated for model validation purposes. The circuit consists of two back-to-back SP8T cartwheel rotary switches, each having four redundant output(input) ports, and four lengths of CPW transmission lines connected in tandem between the non-redundant output(input) ports of the switches. The shortest delay line acts as the 0° reference, whereas three others provide 90°, 180° and 270° of electrical length delay at the 2 GHz centre frequency of operation. The CPW delay lines have space/width/space dimensions of 13/80/13 μm, which then linearly taper down to 7/27/7 μm at the periphery of the switch. The CPW delay line lengths were calculated with Agilent EEsof LineCalc.

Fabrication of the complete phase shifter was based on the same processes as was used for the switch demonstrators, previously described in [2]. Amorphous synthetic quartz was used as the substrate, and the CPW delay lines were made from a base layer of nickel with an overcoat of gold. The assembled phase shifters were mounted on perforated PCBs to provide isolation from the probe station wafer chuck. Furthermore, gold bond wires were employed at all CPW bends, to suppress unwanted slot-line modes and thus avoid introducing additional losses and unwanted ripples into the frequency responses of the phase shifter. A photograph of the phase shifter is shown in Fig. 8.

Measurements of the phase shifter were undertaken using the dc to 8.5 GHz Agilent E5071B vector network analyser (VNA) and Cascade Microtech 9000 RF on-wafer probe station [5]. Bias-Tees and 10 dB attenuators were inserted between the VNA and the probes, as a precaution, to protect the test-set mixers from any unexpected high-voltage transients. The rotors on each switch were rotated in synchronous fashion (one moving clockwise and the other anti-clockwise), using 100 V actuation pulses. This ensured both rotors simultaneously made contact with the same delay line.

The measured insertion and return loss performances for all four phase states (i.e. 0°, 90°, 180° and 270°) are given in Fig. 9. In addition, the insertion loss characteristics for two of the CPW delay lines (i.e. 0° reference and 90°) are also included for comparison. The ripples in the insertion loss frequency response are the result of standing waves caused by the increasing impedance mismatches with frequency from each switch.

© The Institution of Engineering and Technology 2011

doi: 10.1049/iet-map.2010.0132

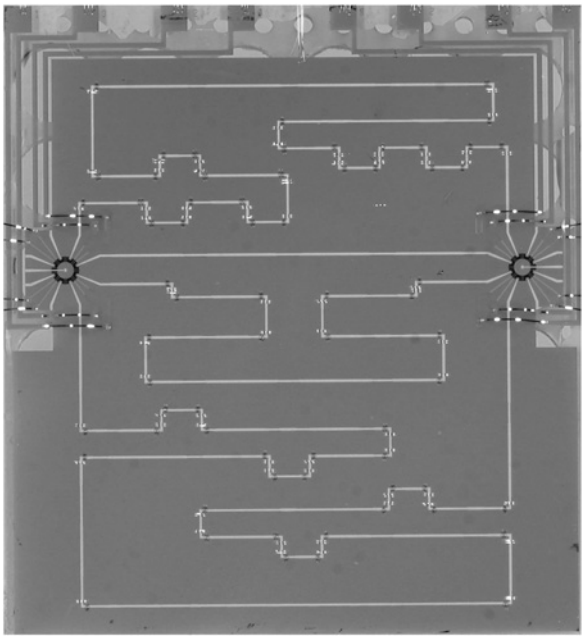

Fig. 8 *Photograph of the of 2.1 × 2.3 cm² TTD phase shifter mounted on PCBs (both rotors have been removed)*

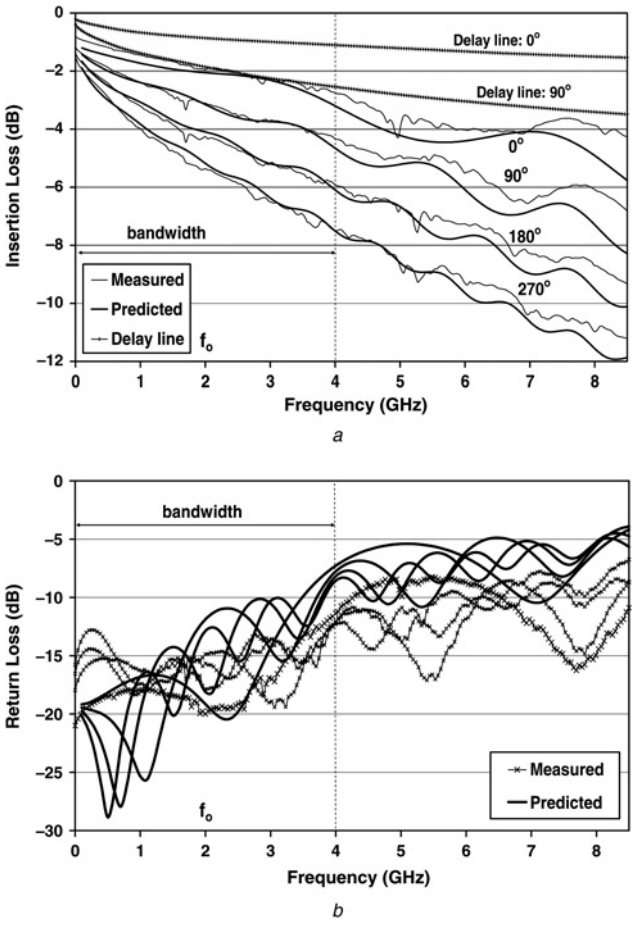

Fig. 9 *Measured and predicted loss responses for the 2 GHz phase shifter*

a Insertion loss
b Return loss

At the 2 GHz centre frequency, there is a minimum insertion loss of around 1.9 dB. The reference line contributes approximately 0.70 dB, with approximately 1.1 dB of additional insertion loss per 90° section of delay line. Including the effects of impedance mismatches, the switches each contribute approximately 0.5 dB of insertion loss, whereas the main input/output CPW feed lines each contribute another 0.075 dB. It is worth stressing that the primary objective of the phase shifter demonstrator was to validate the switch model and not to achieve state-of-the-art performance.

As illustrated in Fig. 9, the relatively high losses for this first prototype demonstrator are dominated by the transmission losses in the delay and feed lines. Therefore this does not represent an inherent limitation for applications of the rotary switch. Several methods could be employed to reduce transmission line losses. For example, the existing 0.5/2 μm-thick nickel/gold material composition for the ground plane could be changed to a much thicker copper/gold composition. The current

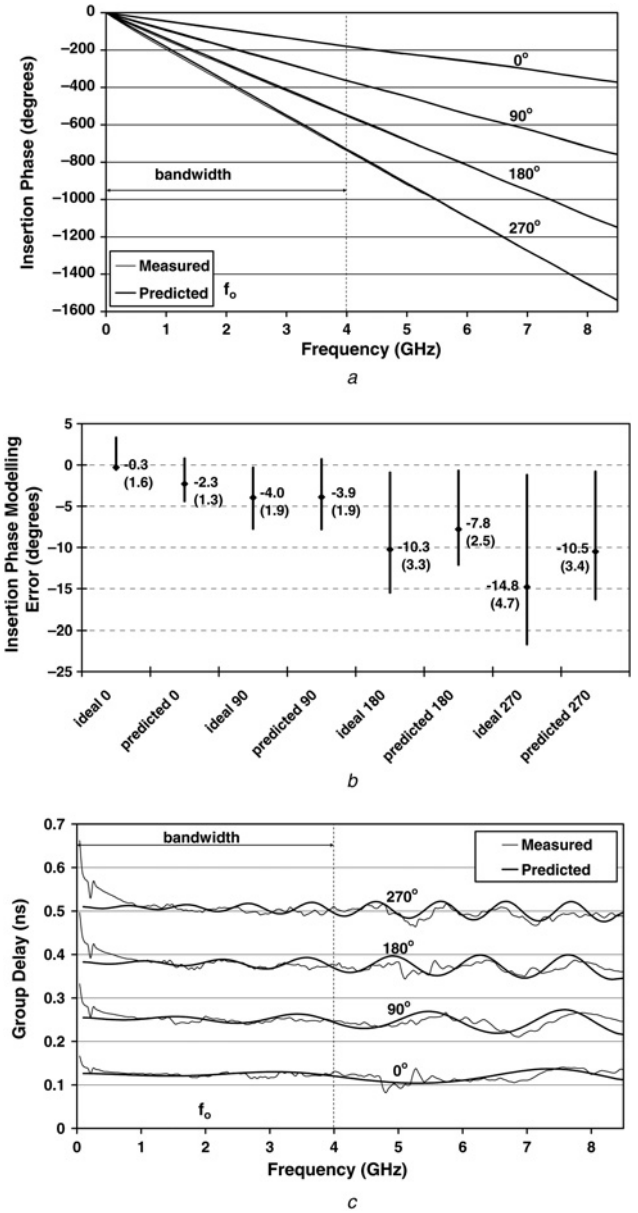

Fig. 10 *Measured and predicted phase responses for the 2 GHz phase shifter*

a Insertion phase (note that the corresponding measured and predicted curves are on top of one another)
b Insertion phase error across the 4 GHz bandwidth for measured-ideal and measured-predicted
c Group delay

© The Institution of Engineering and Technology 2011

thickness of gold corresponds to only one skin depth (1.94 μm) at 2 GHz. Using 3D electromagnetic simulations, described in Section 2.1, it was found that when the material composition of the CPW transmission line is changed from Ni/Au to copper, the insertion loss in dB decreases by approximately a factor of two from dc to 20 GHz. In addition, the electroplating of the signal tracks, associated with the long CPW lines, could be improved to significantly reduce the surface roughness and hence corresponding levels of line attenuation.

The measured and predicted absolute insertion phase angles and differential-phase group delays are given in Fig. 10. Also shown is an analysis of the phase differences between measured data and ideal phase shifter responses, for all four phase states. For the ideal phase shifter, the absolute insertion phase angle for the reference line was locked to the corresponding measured value at 2 GHz. The other values for the ideal response could then be easily calculated for all other frequency points and phase states. The vertical bars in Fig. 10*b* indicate the upper and lower limits of the phase difference for each state, whereas the numbers represent the mean values and below these the corresponding root mean square (RMS) values are given in brackets. It can be seen that the RMS differences in absolute insertion phase, compared to the ideal phase shifter response, increase as 1.6°, 1.9°, 3.3° and 4.7° when the phase states increase from 0°, 90°, 180° to 270°, respectively, across the dc to 4 GHz bandwidth of operation.

4 Predictive equivalent circuit modelling

The previously characterised intrinsic lumped-element equivalent circuit models for the rotary switch and TLINP models for the CPW transmission lines (both described in Section 2), having the same element values, were employed to predict the measured behaviour of the phase shifter. The resulting equivalent circuit model for the complete phase shifter is shown in Fig. 11. Here, the 90°, 180° and 270° delay lines were modelled using multiple sections that correspond to the actual physical meandering of their layouts. Multiple test lines that included varying number of bends were also previously characterised. It was found that bends, having two bond wires at each end to connect the upper grounds together, had no significant effect up to the 8.5 GHz frequency range of the measurement system. As a result, TLINP models with lengths extending to the centre of the bends were used.

The resulting measurement and predictive equivalent circuit model frequency responses for the phase shifter are shown in Figs. 9 and 10 for the loss and phase characteristics, respectively. Very close agreement exists with all the frequency responses, between those measured and generated by the predictive model. It should be noted that no new circuit elements or tweaking of model parameters was needed to achieve this fit.

To evaluate how the measured insertion phase performs against predictions, within the dc to 4 GHz bandwidth of operation, Fig. 10*b* indicates the differences between the two for the three highest phase states. It can be seen that the RMS deviations of insertion phase, from predicted responses, are 1.3°, 1.9°, 2.5° and 3.4° when the phase states increase from 0°, 90°, 180° to 270°, respectively. These low values clearly demonstrate the accuracy of this predictive equivalent circuit modelling.

5 Discussion and conclusions

In this paper, both full 3D electromagnetic and equivalent circuit modelling of an RF MEMS SP8T rotary switch have been described in detail, and reported for the first time. Excellent agreement has been achieved between measurements and modelled performance. Both modelling strategies have given valuable insight into the existing prototype design and scope for optimisation of this unique switch architecture. It has also been shown that the equivalent circuit model is highly effective for designing RF MEMS true delay line phase shifters. To this end, an experimental 2-bit phase shifter having a centre frequency of 2 GHz was demonstrated. The measured loss and phase performance could be accurately predicted from dc to 8.5 GHz using an equivalent circuit model.

Previously, single-pole multiple-throw RF MEMS switches have been realised by integrating a number of single-pole single-throw (SPST) switches [6–9]. However, as the number of bits increases, this solution can result in yield and reliability issues, as noted in [7]. For example, the SP9T switch proposed by Lee *et al.* [9] require 16 times the amount of real estate and has nine separate moving components,

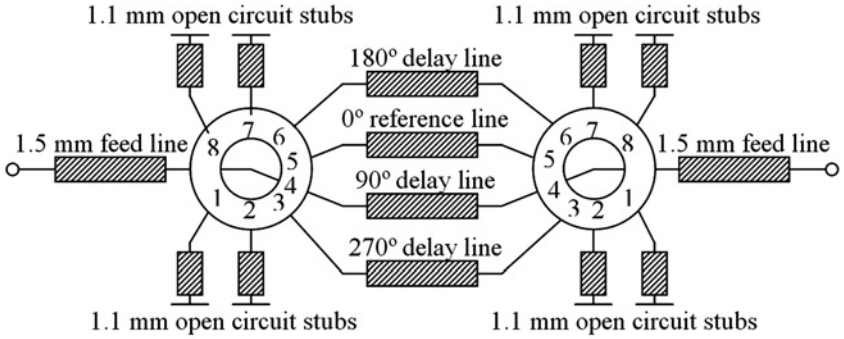

Fig. 11 *Predictive equivalent circuit model of complete 2-bit phase shifter*

© The Institution of Engineering and Technology 2011

doi: 10.1049/iet-map.2010.0132

when compared with our SP8T switch that only has one moving part. Moreover, our switch can tolerate a small increase in the number of throws without an increase in size.

With further optimisation, rotary switches can lead to a more compact and reliable single-pole multi-throw switching solution, when compared with SPST arrays. Even though insertion losses are relatively high with this first prototype demonstrator, this does not represent an inherent limitation for applications of the rotary switch, and various suggestions for the design and fabrication processing improvements have been made to address this issue.

Although the phase shifter described here represents the first ever application of any RF MEMS rotary switch, the authors believe that there is considerable scope for other applications, including reflection-type phase shifters [10], digital attenuators [5] and sectorised antenna array [11].

6 Acknowledgments

The authors would like to express their thanks to Dr. Munir M. Ahmad and Dr. Guodong Hong for help and suggestions during the fabrication processing. We are also grateful for the assistance from Dr. Michael P. Larsson during measurements. This work was partially supported by the UK's Engineering and Physical Sciences Research Council (EPSRC) under Platform Grant EP/E063500/1. This work was also partially supported by Faculty of Engineering, Kasetsart University, under grant 50/16/EE.

7 References

1 Lucyszyn, S. (Ed.): 'Advanced RF MEMS' (Cambridge University Press, Cambridge, UK, 2010)
2 Pranonsatit, S., Holmes, A.S., Robertson, I.D., Lucyszyn, S.: 'Single-pole eight-throw RF MEMS rotary switch', *IEEE J. Microelectromech. Syst.*, 2006, **15**, (6), pp. 1735–1744
3 Dimitrakopoulos, N., Hartley, A., Miles, R.E., Pollard, R.: 'Microwave simulation of an X-band RF MEMS switch'. First EMRS DTC Technical Conf., Edinburgh, UK, A12, 2004
4 Lucyszyn, S.: 'Microwave characterization of nickel', *PIERS Online J.*, 2008, **4**, (6), pp. 686–690
5 Robertson, I.D., Lucyszyn, S. (Eds.): 'RFIC and MMIC design and technology' (IEE, London, UK, 2001)
6 Tan, G.L., Mihailovich, R.E., Hacker, J.B., DeNatale, J.F., Rebeiz, G.M.: 'Low-loss 2- and 4-bit TTD MEMS phase shifters based on SP4 T switches', *IEEE Trans. Microw. Theory Tech.*, 2003, **51**, (1), pp. 297–304
7 Nordquist, C.D., Dyck, C.W., Kraus, G.M., *et al.*: 'A dc to 10 GHz 6-b RF MEMS time delay circuit', *IEEE Microw. Compon. Lett.*, 2006, **16**, (5), pp. 305–307
8 Lee, J., Je, C.H., Kang, S., Choi, C.-A.: 'A low-loss single-pole six-throw switch based on compact RF MEMS switches', *IEEE Trans. Microw. Theory Tech.*, 2005, **53**, (11), pp. 3335–3344
9 Lee, S., Kim, J.-M., Kim, Y.-K., Kwon, Y.: 'A single-pole nine-throw antenna switch using radio-frequency microelectromechanical systems technology for broadband multi-mode and multi-band front-ends', *IoP J. Micromech. Microeng.*, 2008, **18**, (1), pp. 1–8
10 Lucyszyn, S., Robertson, I.D.: 'Analog reflection topology building blocks for adaptive microwave signal processing applications', *IEEE Trans. Microw. Theory Tech.*, 1995, **43**, (3), p. 601–611
11 Pranonsatit, S., Holmes, A.S., Lucyszyn, S.: 'Sectorised horn antenna array using an RF MEMS rotary switch'. Asia-Pacific Microwave Conf., APMC 2010, Yokohama, Japan, December 2010

© The Institution of Engineering and Technology 2011